Bridging Rigidity and Flexibility: Modulation of Supramolecular Hydrogels by Metal Complexation

Oliver S. Stach, Katharina Breul, Christian M. Berač,* Moritz Urschbach, Sebastian Seiffert,* and Pol Besenius*

The combination of complementary, noncovalent interactions is a key principle for the design of multistimuli responsive hydrogels. In this work, an amphiphilic peptide, supramacromolecular hydrogelator which combines metal-ligand coordination induced gelation and thermoresponsive toughening is reported. Following a modular approach, the incorporation of the triphenylalanine sequence FFF into a structural (C_3^{EG}) and a terpyridine-functionalized (C_3^{Tpy}) C_3-symmetric monomer enables their statistical copolymerization into self-assembled, 1D nanorods in water, as investigated by circular dichroism (CD) spectroscopy and transmission electron microscopy (TEM). In the presence of a terpyridine functionalized telechelic polyethylene glycol (PEG) cross-linker, complex formation upon addition of different transition metal ions (Fe^{2+}, Zn^{2+}, Ni^{2+}) induces the formation of soft, reversible hydrogels at a solid weight content of 1 wt% as observed by linear shear rheology. The viscoelastic behavior of Fe^{2+} and Zn^{2+} cross-linked hydrogels are basically identical, while the most kinetically inert Ni^{2+} coordinative bond leads to significantly weaker hydrogels, suggesting that the most dynamic rather than the most thermodynamically stable interaction supports the formation of robust and responsive hydrogel materials.

1. Introduction

The interactions of proteins, enzymes, lipids, and signaling cascades rely on synergistic supramolecular associations whose interplay has been optimized during millions of years of evolution. In natural systems, this commonly includes dissipative processes like the self-organization of microtubuli or actin filaments.[1–3] These biological concepts inspired generations of material scientists to develop a multitude of responsive and adaptive materials based on self-assembling and self-organizing building blocks which interact through noncovalent, reversible interactions.[4,5] Especially the progress achieved in understanding the principles that control the hierarchic ordering and macroscopic functionality on a micro- and mesoscopic level facilitated the rational design of supramolecular synthetic materials with adaptive features.[6–10] One prominent and widely applied approach uses monomeric or polymeric building blocks with hydrophobic and hydrophilic domains whose interplay induces a supramolecular polymerization in aqueous environments.[11–13] The obtained aggregates are stabilized through cooperative, reversible interactions resulting from hydrogen bonding,[14–18] electrostatic,[19–21] or host–guest interactions,[22,23] metal–ligand coordination,[24–26] hydrophobic effects or π–π stacking.[27–31] Note, that multiple hydrogen bonding as well as π–π stackings not only stabilize the supramolecular structures but also induce directed columnar stacks with high aspect ratios.[28,32]

To create responsive materials that are functional in biologically relevant and aqueous environments, peptidic structures are especially suitable due to their well-established and tunable driving force in forming extended, regular superstructures in combination with their excellent biocompatibility, e.g., required for medical applications.[33–36] In this regard, our group previously reported the supramolecular self-assembly of C_3-symmetric dendritic peptide amphiphiles in water which can be controlled through different switches such as charge-screening and redox-reactions.[37–42] Moreover, we have been able to implement thermoresponsive dendritic units into the C_3-symmetric monomers to enable a thermoresponsive hydrogelation.[43] As the engineering of biomimetic materials generally requires the implementation of multistimuli responsive functionalities, such a combination of orthogonal gelation switches remains of great interest. To broaden the scope of multistimuli responsive hydrogels, this work combines the hydrophobic β-sheet driven self-assembly of

O. S. Stach, K. Breul, C. M. Berač, M. Urschbach, S. Seiffert, P. Besenius
Department of Chemistry
Johannes Gutenberg-University Mainz
Duesbergweg 10–14, Mainz 55128, Germany
E-mail: berac@uni-mainz.de; sebastian.seiffert@uni-mainz.de; besenius@uni-mainz.de
K. Breul, C. M. Berač, S. Seiffert, P. Besenius
Graduate School of Materials Science in Mainz
Staudingerweg 9, Mainz 55128, Germany

ADVANCED
SCIENCE NEWS
www.advancedsciencenews.com

{M| acro-
| olecular
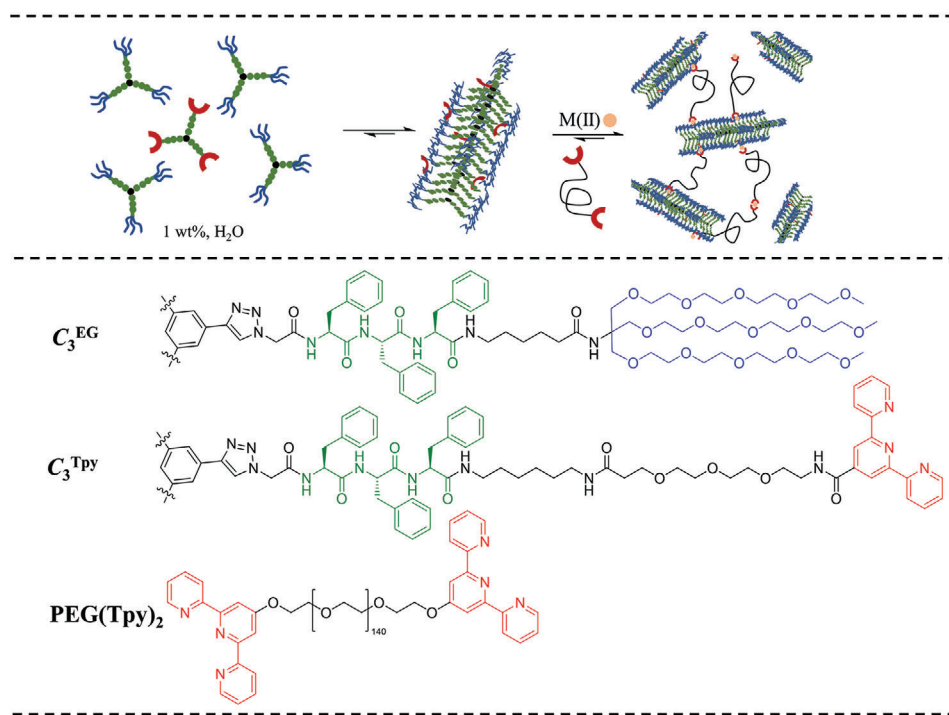Rapid Communications
www.mrc-journal.de

Figure 1. Schematic representation of the transition from the molecularly dissolved structural ($C_3{}^{EG}$) and functional ($C_3{}^{Tpy}$) C_3-symmetric comonomers into 1D nanorods in water and their interconnection with telechelic, terpyridine functionalized polyethylene glycol cross-linkers via metal ion complexation with the corresponding chemical structures of both C_3-symmetric monomers and the telechelic cross-linker.

uncharged peptide amphiphiles and their reversible association using metal–ligand coordination chemistry. Using the tridentate terpyridine ligand offers the advantage of forming highly directional bis-terpyridine complexes with controlled stoichiometry and easily variable complexation strength through the choice of the applied bivalent transition metal ion.[44] In previous studies, the supramolecular association of telechelic polyethylene glycol-terpyridine conjugates has been demonstrated on multiple occasions. However, due to the highly flexible polymer backbone, the formation of hydrogels generally required the use of branched telechelic precursors and high polymer contents around the coil overlap concentration.[45,46] Previous reports have shown that the combination of such flexible linkers with supramolecular structures decreases the critical solid weight content required to induce hydrogelation.[47–52] Following this approach, we designed a multicomponent system that combines the benefits of macromolecular and supramolecular polymers by interconnecting rigid, self-assembled peptide 1D nanostructures with flexible, telechelic polyethylene glycol (PEG) chains through the reversible complexation of terpyridine ligands with Zn^{2+}, Fe^{2+}, and Ni^{2+}.[53] To incorporate terpyridine (Tpy) groups into 1D nanorods, a previously reported modular approach is applied, using β-sheet encoded statistical supramolecular copolymerization of FFF-containing, structural monomers. Such a copolymerization strategy relies on the incorporation of functional comonomers and yields surface decorated anisotropic nanostructures, with a tunable density of ligands and cross-linking moieties.[54]

2. Results and Discussion

A terpyridine bearing C_3-symmetric peptide monomer $C_3{}^{Tpy}$ **12** (**Figure 1**) was synthesized starting from *tert*-butyl[tri(ethylene glycol) propionate] (**1**) (Scheme S1, Supporting Information). After activation with methanesulfonyl chloride, nucleophilic substitution with sodium azide and a consecutive Staudinger reduction, [2,2′:6′,2″-terpyridine]-4′-carboxylic acid (**6**) was attached to this hydrophilic linker via an amide coupling. Standard acidic cleavage of the *tert*-butyl group yielded the Tpy-functionalized linker **7**. The structure defining oligopeptide sequence N₃-GFFF-OH **8** was synthesized by solid-phase peptide synthesis and coupled with *N*-Boc-1,6-hexane amine hydrochloride **9** in a PyBOP-mediated amidation. The resulting peptide **10** was attached to 1,3,5-triethynylbenzene in a Cu¹-catalyzed azide-alkyne cycloaddition (CuAAC). The C_3-symmetric scaffold **11** was obtained after removal of the *tert*-butyl group under acidic conditions and finally attached to the Tpy linker **7** to give the Tpy-functionalized monomer $C_3{}^{Tpy}$ **12**. To obtain a structural comonomer, a two-step synthesis was performed starting from the previously reported Newkome-type dendron **13** and the oligopeptide sequence N₃-GFFF-OH (**8**).[42] Attachment of the peptide amphiphile **14** to 1,3,5-triethynylbenzene yielded $C_3{}^{EG}$ **15** (Figure 1, Scheme S2, Supporting Information).

Due to the successful application in a previous study with a focus on structural and functional C_3-symmetric comonomers with peptidic FFF sequences, it appeared promising to incorporate the Tpy monomers through a statistical supramolecular
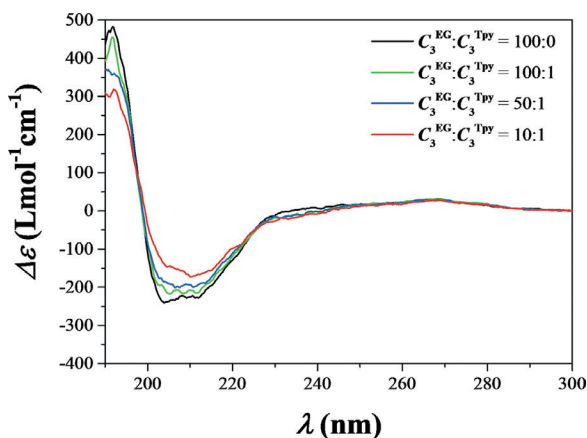
**ADVANCED
SCIENCE NEWS**

www.advancedsciencenews.com

[M]acro-molecular
Rapid Communications

www.mrc-journal.de

Figure 2. Circular dichroism spectroscopic investigation of the self-assembly of C_3^{EG} and C_3^{Tpy}: Pure C_3^{EG} (black) and $C_3^{EG}:C_3^{Tpy}$ mixtures in ratios of 100:1 (green), 50:1 (blue), and 10:1 (red) ($c = 50 \times 10^{-6}$ M, water).

copolymerization (Figure 1).[54] An initial indication for the successful copolymerization of both monomers was the observed transition from turbid suspensions of pure C_3^{Tpy} in water to transparent solutions when mixed with C_3^{EG}. Further on, we used circular dichroism (CD) spectroscopy to investigate the supramolecular copolymerization of the monomers in water at ratios of $C_3^{EG}:C_3^{Tpy} = 100:1$, 50:1, and 10:1 (**Figure 2**).

The CD spectrum of pure C_3^{EG} in water serves as reference for all further comparisons and displays strong negative bands at $\lambda = 204$ and 211 nm, which can be identified as characteristic signals for the formation of β-sheet secondary structures (Figure 2). In addition to the representative β-sheet indicating signals, weak positive bands at $\lambda = 265$ and 270 nm appeared, which belong to the aromatic benzene tris(triazole) moiety from the hydrophobic monomer core.[42] While no shift of the signal was observed, the copolymers with ratios of 100:1 ($\Delta\varepsilon = -204$ L mol^{-1} cm^{-1}, green) and 50:1 ($\Delta\varepsilon = -186$ L mol^{-1} cm^{-1}, blue) revealed weaker intensities of the characteristic β-sheet bands at $\lambda = 204$ nm in comparison to the pure C_3^{EG} solution ($\Delta\varepsilon = -241$ L mol^{-1} cm^{-1}, black). When the amount of the Tpy-monomer is increased to 10%, an even more pronounced intensity decrease of the negative and positive bands is noticeable ($\Delta\varepsilon = -140$ L mol^{-1} cm^{-1}). These results are independent of the monomer concentration (Figures S2–S4, Supporting Information), which, together with the transition of turbid suspensions of C_3^{Tpy} to clear solutions of both monomers, indicates the successful copolymerization of both monomers in water. The decreasing band intensity at higher Tpy-monomer ratios is indicative of competing interactions of the hydrophobic Tpy moieties with the hydrophobic FFF tripeptide structural motif.

To probe this hypothesis, transmission electron microscopy (TEM) images were recorded to characterize the morphology of the supramolecular homo- and copolymers in water (**Figure 3**A,B). While anisotropic 1D nanorods are formed in both cases, the average length of the nanostructures formed in pure C_3^{EG} solutions ($L_n = 94 \pm 58$ nm) is significantly larger than that of the $C_3^{EG}:C_3^{Tpy} = 10:1$-copolymer ($L_n = 40 \pm 16$ nm) which supports the assumption of competing interactions and interference with monomer stacking at higher Tpy-contents.

Once the supramolecular copolymerization of both monomers was confirmed, the anticipated metal-induced cross-linking of the described nanorods was investigated. To characterize the hydrogelation and viscoelastic properties of the resulting networks, shear rheological measurements were performed at a total monomer concentration of 1 wt% and a comonomer ratio of $C_3^{EG}:C_3^{Tpy} = 10:1$. After sonication for 5 min and equilibration for 24 h, amplitude sweeps ($\gamma = 0.01$–100%) were conducted at a constant frequency of $\omega = 1\%$ ($T = 20$ °C).

To firstly address the question, if and under which conditions a gelation is possible, Fe^{2+} was chosen as cross-linking metal ion as it rapidly forms thermodynamically and kinetically stable bis-terpyridine complexes ($\log(k_{ass}) = 4.9$, $\log(k_{dis}) = -2.2$, $\log K = 20.9$).[55] However, as shown in **Figure 4**A, the addition of a stoichiometric amount of Fe^{2+} (Fe^{2+}:Tpy = 1:2) to the pure comonomer mixture only leads to a slightly increased solution viscosity whereas no viscoelastic plateau emerges. Only after addition of the flexible, Tpy-functionalized PEG cross-linker **18** ($n_{Tpy}(\textbf{PEG(Tpy)}_2) = n_{Tpy}(C_3^{Tpy})$ and thus $n(\textbf{PEG(Tpy)}_2) = 3/2\, n(C_3^{Tpy})$), a weak hydrogel with a plateau modulus of $G_N^0 = 16$ Pa and a considerable dissipation factor ($\tan\delta = G'/G''$) is formed within a linear viscoelastic (LVE) regime reaching from $\gamma = 0.01\%$ to 5%.

To investigate how the gel properties depend on the Tpy cross-linking reaction, the thermodynamic and kinetic stability of the complexation was next varied through the choice of the applied metal ion. In case of the kinetically less stable and weaker Zn^{2+}-complex ($\log(k_{ass}) = 6.1$, $\log(k_{dis}) = -0.1$, $\log K = 6$),[55] a similar plateau modulus but a smaller dissipation factor and lower flow point ($G' = G''$) are observed in comparison to the Fe^{2+} cross-linked hydrogel as shown in Figure 4B. Apparently, the different association strengths and average dissociation times (1.3 s – Zn^{2+}; 160 s – Fe^{2+}) of these bis(Tpy)-complexes do not significantly affect the extent of cross-linking on the investigated time scale. This observation is consistent with the initially hypothesized metal-induced cross-linking of the pre-assembled 1D nanorods. The complexation seems to switch on hydrogelation, however the ultimate viscoelasticity is not limited by the Tpy complexation and its binding kinetics or strength. The most likely limiting factor is thus rather the dynamic assembly and dis-assembly of the nanorods themselves. To provide further proof for this binding scenario, we performed a control experiment with an over stochiometric amount of Zn^{2+} (Figure 4B). The equilibrium of the Zn^{2+}-terpyridine complexation can be shifted towards the thermodynamically less stable monocomplex in the presence of an excess of the metal ion which should impede the efficient interconnection of the 1D nanorods.[56] As anticipated, the respective amplitude sweep (Figure 4B, ◆) does not show any viscoelastic plateau but resembles that of the plain comonomer solution.

Further on, we investigated the hydrogel formation upon addition of stronger complexing Ni^{2+} ions (Figure 4B, ●) which form the most kinetically inert complexes with average dissociation times in the range of hours ($\log(k_{ass}) = 3.1$, $\log(k_{dis}) = -7.6$, $\log K = 21.8$).[55] Due to the high association constant, reversible polymer networks cross-linked by bis(Tpy)-Ni^{2+} complexes show purely elastic behavior at room temperature[57] and typical network relaxation times measurable by stress relaxation experiments at elevated temperatures (70 °C) comprise more than
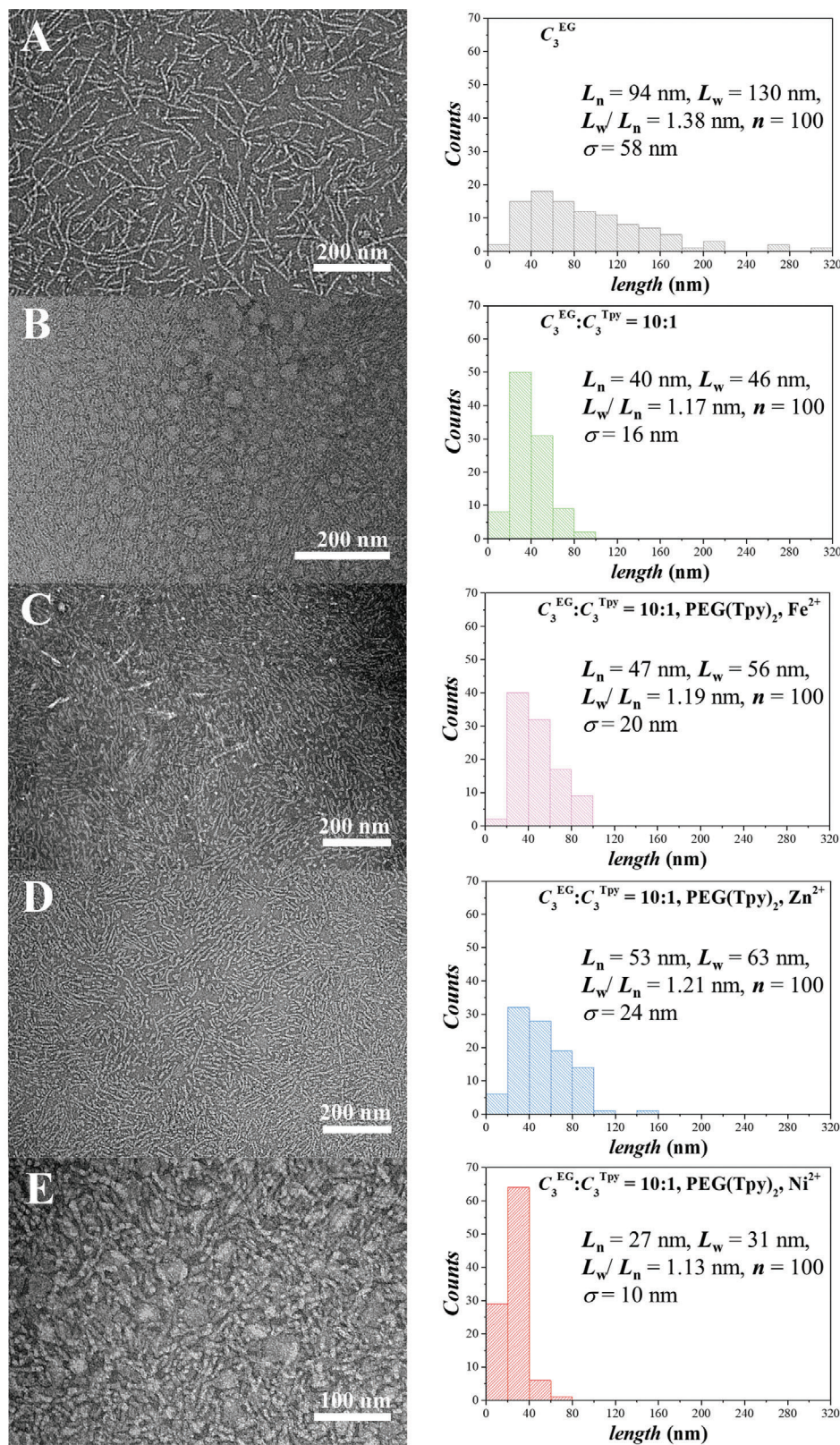
Figure 3. Negative stained transmission electron microscopy micrographs with the corresponding histograms of aqueous solutions of A) C_3^{EG}, B) $C_3^{EG}:C_3^{Tpy}$ (10:1), C) $C_3^{EG}:C_3^{Tpy}$ (10:1), PEG(Tpy)$_2$ and Fe^{2+}, D) $C_3^{EG}:C_3^{Tpy}$ (10:1), PEG(Tpy)$_2$ and Zn^{2+}, and E) $C_3^{EG}:C_3^{Tpy}$ (10:1), PEG(Tpy)$_2$ and Ni^{2+} ($c = 25 \times 10^{-6}$ M, water, 20 °C). Note, that all metal ions were added in form of their respective triflate salts.
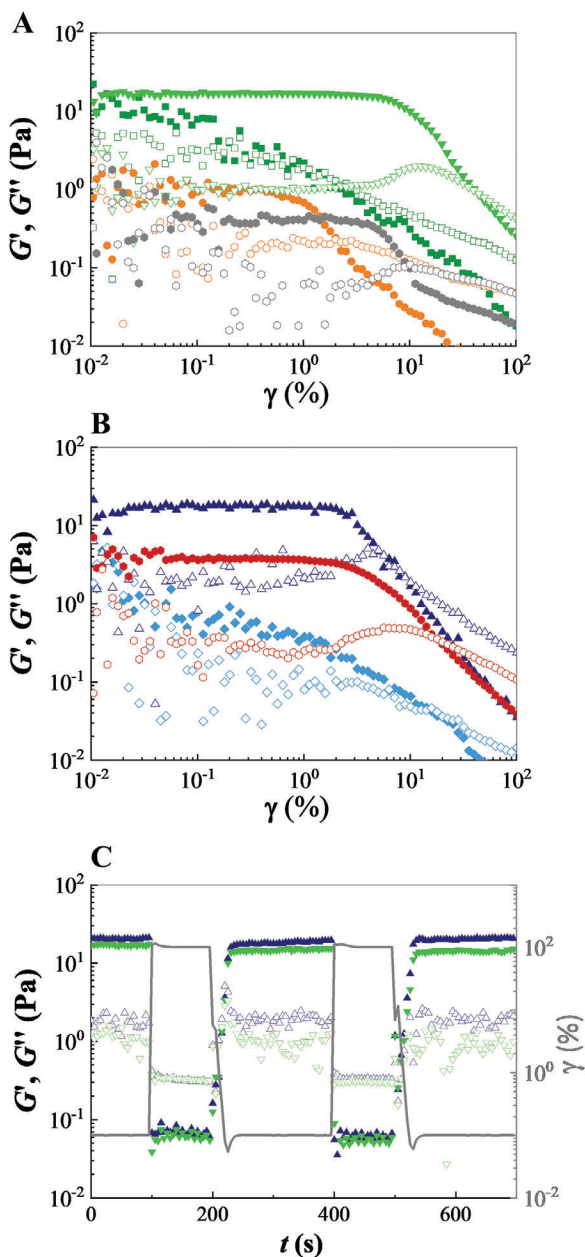
Figure 4. Oscillatory-shear amplitude-sweeps of aqueous solutions of C_3^{EG}:C_3^{Tpy} = 10:1 mixtures (1 wt%) in the presence of A) no further components (●), **PEG(Tpy)$_2$** (●), only C_3^{EG} (●), Fe^{2+} (■), Fe^{2+} and **PEG(Tpy)$_2$** (▼) and B) Zn^{2+} and **PEG(Tpy)$_2$** (▲), Ni^{2+} and **PEG(Tpy)$_2$** (●) and **PEG(Tpy)$_2$** together with an over-stoichiometric amount of Zn^{2+} (◆). C) Step strain measurements (same color code as before) (M^{2+}:Tpy = 1:2 if not indicated otherwise, ω = 1 rad s^{-1}, H$_2$O, 20 °C, G': full symbols, G'': empty symbols). Note, that all metal ions were added in form of their respective triflate salts.

15 h.[58] However, in the present study, a lower plateau modulus but similar LVE regime was observed in comparison to the Fe^{2+} and Zn^{2+} cross-linked gels. The nanostructural investigation of the Ni^{2+} cross-linked nanorods via TEM revealed not only a decrease in the average length compared to the other metal ion

treated samples (Fe^{2+}: L_n = 47 ± 20 nm; Zn^{2+}: L_n = 53 ± 24 nm; Ni^{2+}: L_n = 27 ±10 nm), but also a significantly increased number of clusters (Figure 3E). This is indicative for the formation of larger nanorod bundles which reduces the number of elastically active components. It appears likely that the practically covalent binding of the terpyridine functionalized comonomers to each other or the PEG linker prohibits the dynamic dis- and reassembly of the anisotropic nanostructures which are essential for the viscoelasticity of this highly dilute system. Note also, that we have already shown that telechelic terpyridine bearing PEG conjugates do not form hydrogels at such low concentrations of 1 wt%.[45]

To probe the reversible nature of the noncovalent networks, step-strain tests were conducted (Figure 4C). Under high strain conditions (γ = 100%), the microstructure undergoes disruption, leading to a liquid-like state with $G' < G''$. After removal of the strain (γ = 1%), an immediate transition to the initial status is observed as the microstructure regenerates. Such behavior was observed for at least two cycles of testing, demonstrating the rapid self-healing characteristics of these metallo-supramolecular hydrogels.

Finally, considering the formerly described thermoresponsive properties of related C_3-symmetric monomers with dendritic oligo(ethylene glycol) moieties, temperature-dependent CD measurements were performed using the 10:1 monomer mixture between 10 °C and 90 °C (**Figure 5**A, Figure S5–S7, Supporting Information). As shown in Figure 5A, the position, shape, and intensity of the characteristic CD bands does not alter significantly upon increasing the temperature. However, while still showing the presence of β-sheet structures, plotting the signal intensity at λ = 210 nm against the temperature shows a 10% decrease in the signal intensity from $\Delta\epsilon = -165$ L mol^{-1} cm^{-1} at 10 °C to $\Delta\epsilon = -148$ L mol^{-1} cm^{-1} at 90 °C (Figure S5, Supporting Information).

Therefore, the influence of temperature on the viscoelastic properties was also examined (Figure 5B). The plain comonomer mixture, as well as the Fe^{2+} and Zn^{2+} cross-linked samples containing **PEG(Tpy)$_2$**, display a parallel increase of storage and loss modulus when the temperature is raised from 20 °C to 50 °C. In case of the plain comonomer solution, G' increases from ≈0.1 to 2 Pa which can be explained by the decreasing hydrophilicity of the oligo-ethylene glycol corona at elevated temperatures and most likely leads to weak network formation via clustering of the nanorods. This effect is much more pronounced when using the Zn^{2+} and Fe^{2+} cross-linked hydrogels, where the temperature-dependent protocol leads to significant toughening and an increase of the storage moduli by more than one order of magnitude between 20 °C and 50 °C (Figure 5B).

3. Conclusion

In summary, we have presented the synthesis and application of a terpyridine decorated supramolecular copolymer, using C_3-symmetric, β-sheet driven self-assembling triphenylalanine domains (FFF). The copolymerization of the structural C_3^{EG} and the functional C_3^{Tpy} monomers in water was investigated via CD and TEM images and revealed weaker intensities and shorter 1D nanorods for the corresponding Tpy-functional copolymers in comparison to the pure C_3^{EG}. The incorporation of the terpyridine bearing functional monomer C_3^{Tpy} allowed to cross-link the 1D nanorods through a flexible, telechelic PEG linker by
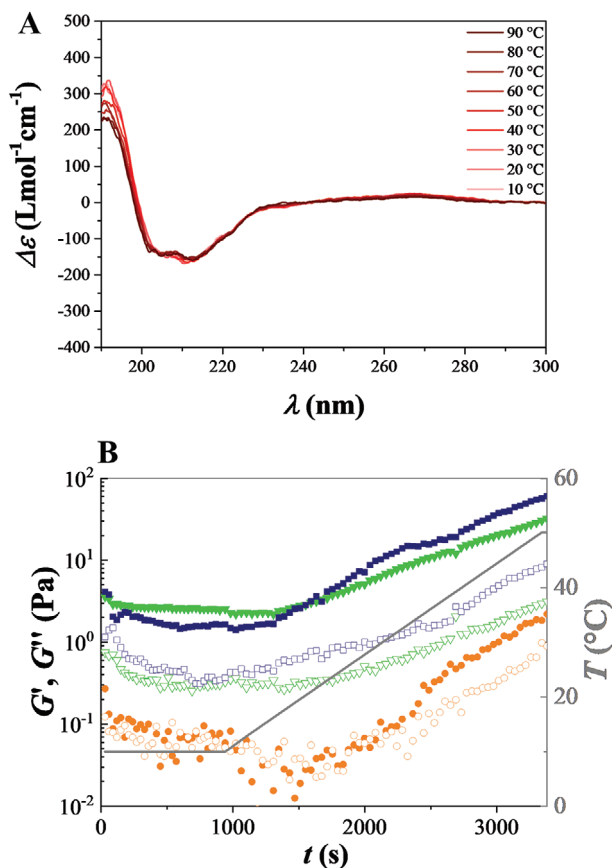
**ADVANCED
SCIENCE NEWS**

www.advancedsciencenews.com

{M}acro-
molecular
Rapid Communications

www.mrc-journal.de

Figure 5. Temperature-dependent investigation of aqueous solutions of C_3^{EG}:C_3^{Tpy} = 10:1 mixtures. A) Circular dichroism (CD) spectra with a stepwise temperature increase from 10 °C to 90 °C ($c = 50 \times 10^{-6}$ M). B) Temperature-dependent oscillatory time sweep (1 wt%, γ = 1%, ω = 1 Hz, G': full symbols, G'': empty symbols) in the presence of no further components (●), Fe^{2+} and **PEG(Tpy)$_2$** (▼), Zn^{2+} and **PEG(Tpy)$_2$** (■).

metal-induced coordination. TEM imaging revealed the formation of smaller nanorods and clusters while the metal-induced hydrogelation could be shown in rheological measurements. Interestingly, no significant differences were observed between the viscoelastic properties of Fe^{2+} and Zn^{2+} cross-linked gels (G' = 16 Pa) while the cross-linking through the kinetically mostly inert Ni^{2+} complexes led to significantly weaker hydrogels (G' = 5 Pa). Moreover, thermoresponsive behavior with a significant increase of the gel strength by one order of magnitude between 20 °C and 50 °C was shown by thermorheological measurements. Within this work, we have tuned our C_3-symmetric modular system to incorporate an insoluble, functional comonomer into a supramolecular structure which could be used to cross-link the soluble supra-structures to yield metal coordination induced soft and reversible hydrogels.

4. Experimental Section

CD spectroscopy was performed on a Jasco J-815 spectrometer with the software Spectra Manager v2.12.00. All samples were baseline corrected and measured, using a 110-QS Suprasil quartz glass cuvettes

with a path length of 2 mm at varying temperature, controlled by a Jasco PTC-423S/15 peltier element. For prevention of noise increasement, all concentrations were adjusted to keep the photomultipliers high voltage (HV) value below 600 V at the respective wavelength area of interest (λ > 190 nm). Each sample was measured at least three times and averaged to minimize further errors.

TEM images were recorded on a *Tecnai* T12 system by Fei, equipped with a BioTWIN lens and a LaB_6 cathode, operating at 120 kV. The digital electron micrographs were recorded with a 4k x 4k *Cmos* camera by TVIPS and the received images were analyzed with the processing application ImageJ. A glow-discharged CF300-CU copper grid by Electron Microscopy Sciences, coated with a 3–4 nm carbon layer, was used by adsorbing 5 µL of the sample for 2 min. Negative staining was performed by using 5 µL of a 2 wt% solution of uranyl acetate for 1 min. An excess of liquid was removed with Whatman grade 4 filter papers by GE Healthcare Bio-Sciences. Length characterization of the rod-like nanostructures was performed by using the software ImageJ 1.53i (Wayne Rasband National Institutes of Health, USA).

Rheological studies were performed on a stress-controlled MCR 302 rheometer by Anton Paar equipped with a stainless-steel cone-plate geometry (cone angle: 1°; cone diameter: 25 mm) and a solvent trap. Inertial calibration was performed prior to each measurement.

Samples were prepared from stock solutions of each monomer dissolved in DMSO, and stock solutions of telechelic cross-linker and the respective metal salts, each dissolved in water. After mixing, the monomers were lyophilized consecutively from DMSO and water. The lyophilizate was dissolved in water again, before the appropriate volumina of a PEG(Tpy)$_2$ and a metal salt solution were added. After addition of the metal salt, the samples were sonicated for 5 min and further equilibrated for 24 h at r.t. Afterwards, 80−100 µL of the solutions were placed on the lower rheometer plate using an Eppendorf pipette. Next, all occurring air bubbles were removed with the pipette tip. The upper geometry was lowered onto the sample and any excess amount of the sample was removed using a paper wipe. All samples underwent conditioning and were monitored for 30 min at a constant shearing amplitude and frequency (γ = 0.01%; ω = 1 rad s^{-1}) to ensure sample equilibration before amplitude- and temperature-sweeps were recorded. Further experimental details can be found in the Supporting Information.

All data were processed by using the software Origin v9.0 by OriginLab Corporation.

Supporting Information

Supporting Information is available from the Wiley Online Library or from the author.

Acknowledgements

Conflict of Interest

The authors declare no conflict of interest.

Data Availability Statement

Research data are not shared.

[1] M. Kirschner, *Cell* **1986**, *45*, 329.
[2] D. A. Fletcher, R. D. Mullins, *Nature* **2010**, *463*, 485.
[3] R. Merindol, A. Walther, *Chem. Soc. Rev.* **2017**, *46*, 5588.
[4] F. Xia, L. Jiang, *Adv. Mater.* **2008**, *20*, 2842.
[5] U. G. K. Wegst, H. Bai, E. Saiz, A. P. Tomsia, R. O. Ritchie, *Nat. Mater.* **2015**, *14*, 23.
[6] J.-M. Lehn, *Science* **2002**, *295*, 2400.
[7] G. M. Whitesides, *Science* **2002**, *295*, 2418.
[8] E. Mattia, S. Otto, *Nat. Nanotechnol.* **2015**, *10*, 111.
[9] B. A. Grzybowski, W. T. S. Huck, *Nat. Nanotechnol.* **2016**, *11*, 585.
[10] G. Vantomme, E. W. Meijer, *Science* **2019**, *363*, 1396.
[11] L. Brunsveld, B. J. B. Folmer, E. W. Meijer, R. P. Sijbesma, *Chem. Rev.* **2001**, *101*, 4071.
[12] T. Aida, E. W. Meijer, S. I. Stupp, *Science* **2012**, *335*, 813.
[13] P. Besenius, *J. Polym. Sci., Part A: Polym. Chem.* **2017**, *55*, 34.
[14] R. P. Sijbesma, F. H. Beijer, L. Brunsveld, B. J. B. Folmer, J. H. K. K. Hirschberg, R. F. M. Lange, J. K. L. Lowe, E. W. Meijer, *Science* **1997**, *278*, 1601.
[15] B. J. B. Folmer, R. P. Sijbesma, R. M. Versteegen, J. A. J. Van Der Rijt, E. W. Meijer, *Adv. Mater.* **2000**, *12*, 874.
[16] P. Cordier, F. Tournilhac, C. Soulié-Ziakovic, L. Leibler, *Nature* **2008**, *451*, 977.
[17] W. L. Jorgensen, J. Pranata, *J. Am. Chem. Soc.* **1990**, *112*, 2008.
[18] J. Pranata, S. G. Wierschke, W. L. Jorgensen, *J. Am. Chem. Soc.* **1991**, *113*, 2810.
[19] L. Wang, C. Gong, X. Yuan, G. Wei, *Nanomaterials* **2019**, *9*, 285.
[20] M. F. Hagan, *Adv. Chem. Phys.* **2014**, *155*, 1.
[21] W. K. Kegel, P. Van Der Schoot, *Biophys. J.* **2006**, *91*, 1501.
[22] G. Li, L. B. Mcgown, *Science* **1994**, *264*, 249.
[23] V. Serreli, C.-F. Lee, E. R. Kay, D. A. Leigh, *Nature* **2007**, *445*, 523.
[24] G. R. Whittell, M. D. Hager, U. S. Schubert, I. Manners, *Nat. Mater.* **2011**, *10*, 176.
[25] T. Rossow, S. Bayer, R. Albrecht, C. C. Tzschucke, S. Seiffert, *Macromol. Rapid Commun.* **2013**, *34*, 1401.
[26] T. Rossow, S. Seiffert, *Polym. Chem.* **2014**, *5*, 3018.
[27] L. A. Cuccia, J.-M. Lehn, J.-C. Homo, M. Schmutz, *Angew. Chem., Int. Ed.* **2000**, *39*, 233.
[28] M. Hartlieb, E. D. H. Mansfield, S. Perrier, *Polym. Chem.* **2020**, *11*, 1083.
[29] F. J. M. Hoeben, P. Jonkheijm, E. W. Meijer, A. P. H. J. Schenning, *Chem. Rev.* **2005**, *105*, 1491.
[30] C. R. Martinez, B. L. Iverson, *Chem. Sci.* **2012**, *3*, 2191.
[31] Z. Chen, A. Lohr, C. R. Saha-Möller, F. Würthner, *Chem. Soc. Rev.* **2009**, *38*, 564.
[32] S. Xian, M. J. Webber, *J. Mater. Chem. B* **2020**, *8*, 9197.
[33] H. Cui, M. J. Webber, S. I. Stupp, *Biopolymers* **2010**, *94*, 1.
[34] K. Sato, M. P. Hendricks, L. C. Palmer, S. I. Stupp, *Chem. Soc. Rev.* **2018**, *47*, 7539.
[35] J. Boekhoven, S. I. Stupp, *Adv. Mater.* **2014**, *26*, 1642.
[36] S. I. Stupp, *Adv. Mater.* **2020**, *32*, 1906741.
[37] R. Appel, J. Fuchs, S. M. Tyrrell, P. A. Korevaar, M. C. A. Stuart, I. K. Voets, M. Schönhoff, P. Besenius, *Chem. - Eur. J.* **2015**, *21*, 19257.
[38] P. Ahlers, H. Frisch, P. Besenius, *Polym. Chem.* **2015**, *6*, 7245.
[39] P. Ahlers, H. Frisch, D. Spitzer, Z. Vobecka, F. Vilela, P. Besenius, *Chem. - Asian J.* **2014**, *9*, 2052.
[40] H. Frisch, Y. Nie, S. Raunser, P. Besenius, *Chem. - Eur. J.* **2015**, *21*, 3304.
[41] R. Van Buel, D. Spitzer, C. M. Berac, P. Van Der Schoot, P. Besenius, S. Jabbari-Farouji, *J. Chem. Phys.* **2019**, *151*, 014902.
[42] C. M. Berac, L. Zengerling, D. Straßburger, R. Otter, M. Urschbach, P. Besenius, *Macromol. Rapid Commun.* **2020**, *41*, 1900476.
[43] D. Spitzer, L. L. Rodrigues, D. Straßburger, M. Mezger, P. Besenius, *Angew. Chem., Int. Ed.* **2017**, *56*, 15461.
[44] P. R. Andres, U. S. Schubert, *Adv. Mater.* **2004**, *16*, 1043.
[45] W. Schmolke, M. Ahmadi, S. Seiffert, *Phys. Chem. Chem. Phys.* **2019**, *21*, 19623.
[46] M. F. Koziol, K. Fischer, S. Seiffert, *Macromolecules* **2021**, *54*, 4375.
[47] E. Vereroudakis, M. Bantawa, R. P. M. Lafleur, D. Parisi, N. M. Matsumoto, J. W. Peeters, E. Del Gado, E. W. Meijer, D. Vlassopoulos, *ACS Cent. Sci.* **2020**, *6*, 1401.
[48] M. J. Glassman, J. Chan, B. D. Olsen, *Adv. Funct. Mater.* **2013**, *23*, 1182.
[49] W. E. M. Noteborn, D. N. H. Zwagerman, V. S. Talens, C. Maity, L. Van Der Mee, J. M. Poolman, S. Mytnyk, J. H. Van Esch, A. Kros, R. Eelkema, R. E. Kieltyka, *Adv. Mater.* **2017**, *29*, 1603769.
[50] R. E. Kieltyka, A. C. H. Pape, L. Albertazzi, Y. Nakano, M. M. C. Bastings, I. K. Voets, P. Y. W. Dankers, E. W. Meijer, *J. Am. Chem. Soc.* **2013**, *135*, 11159.
[51] M. M. E. Koenigs, A. Pal, H. Mortazavi, G. M. Pawar, C. Storm, R. P. Sijbesma, *Macromolecules* **2014**, *47*, 2712.
[52] A. V. Zhukhovitskiy, M. Zhong, E. G. Keeler, V. K. Michaelis, J. E. P. Sun, M. J. A. Hore, D. J. Pochan, R. G. Griffin, A. P. Willard, J. A. Johnson, *Nat. Chem.* **2016**, *8*, 33.
[53] R. Eelkema, A. Pich, *Adv. Mater.* **2020**, *32*, 1906012.
[54] D. Straßburger, N. Stergiou, M. Urschbach, D. Yurugi, D. Spitzer, D. Schollmeyer, E. Schmitt, P. Besenius, *ChemBioChem* **2018**, *19*, 912.
[55] R. H. Holyer, C. D. Hubbard, S. F. A. Kettle, R. G. Wilkins, *Inorg. Chem.* **1966**, *5*, 622.
[56] R. Dobrawa, P. Ballester, C. R. Saha-Möller, F. Würthner, *Metal-Containing and Metallo-Supramolecular Polymers and Materials (ACS Symposium Series, No. 928)*, American Chemical Society, USA **2006**.
[57] M. Ahmadi, S. Seiffert, *J. Polym. Sci.* **2020**, *58*, 330.
[58] I. Mahmad Rasid, J. Ramirez, B. D. Olsen, N. Holten-Andersen, *Phys. Rev. Mater.* **2020**, *4*, 55602.